Available online at www.sciencedirect.com

ScienceDirect

Procedia CIRP 65 (2017) 7 – 12

www.elsevier.com/locate/procedia

3rd CIRP Conference on BioManufacturing

The effect of cooling strategies and machining feed rate on the corrosion behavior and wettability of AZ31 alloy for biomedical applications

R. Bertolini*[a], S. Bruschi[a], A. Ghiotti[a], L. Pezzato[a], M. Dabalà[a]

[a]*Dept. Of Industrial Engineering, University of Padova, Via Venezia 1, 35131, Padova, Italy*

* Corresponding author. Tel.: +39 049 8276819; fax: +39-049-8276819. *E-mail address:* rachele.bertolini@dii.unipd.it

Abstract

In this work, the corrosion rate of the AZ31 magnesium alloy in physiological environment was improved by optimized machining process parameters. Cryogenic turning was exploited to obtain a featureless layer in the machined sub-surface, while the feed rate was modified to reduce the aspect ratio of the feed marks characteristic of the turning operation, achieving a decrease of the alloy wettability. The obtained results showed that the aforementioned combined aspects acted as an efficient strategy to enhance the AZ31 poor corrosion behavior, which represents the major obstacle of its effective application in the biomedical field.

Peer-review under responsibility of the scientific committee of the 3rd CIRP Conference on BioManufacturing 2017

Keywords: AZ31 alloy; biomaterials; cryogenic machining; corrosion behaviour; wettability.

1. Introduction

Magnesium alloys are emerging as potential candidates for degradable temporary implants because of their mechanical properties that are closer to those of the natural bone compared to other metals, their good biocompatibility, nontoxicity and biodegradability. However, once placed in the human body, they tend to corrode too quickly, loosening their structural stability before the end of the period of complete healing. Therefore, the rapid degradation in physiological environment limits the clinical applications of these alloys to a great extent. In recent years, the research studies dealing with clinical applications of the magnesium alloys have been mainly concerned on reducing their corrosion degradation rate. The surface characteristics of the implant in particular play a fundamental role in governing the corrosion resistance and they can be suitably modified through Severe Plastic Deformation (SPD) processes [1].

Sunil et al. [2] studied the influence of a four passes Equal Channel Angular Pressing (ECAP) process on the corrosion behavior of the AZ31 magnesium alloy, demonstrating that such technique led to the formation of a refined microstructure, which induced a better degradation behavior compared to the annealed state. Denkena et al. [3] exploited the deep rolling technique in order to induce a compressive residual state on the subsurface layer of a MgCa3.0 magnesium alloy, achieving, in this way, an enhancement in the alloy corrosion resistance. Dinesh et al. [4] studied the influence of the cooling strategy on the cutting forces, cutting temperatures and surface integrity of the ZK60 magnesium alloy; they found that cryogenic machining led to a reduction in the cutting forces and cutting temperature, as well as guaranteed an improved surface integrity compared to dry cutting. Zhang et al. [5] studied the influence of roller burnishing on the cyclic fatigue life performances of an AZ80 magnesium alloy; they demonstrated that an improvement in the fatigue strength up to 110% compared to the initial workpiece was achieved.

However, only few studies were aimed at investigating the effect of the machining-induced microstructure on the corrosion behavior and, above all, in none of them the reduction in wettability was used as a strategy for obstructing the degradation phenomena.

To this aim, the objective of the present work is to investigate the effect of different machining parameters, namely the cooling strategy and feed rate, on the degradation behavior

Peer-review under responsibility of the scientific committee of the 3rd CIRP Conference on BioManufacturing 2017
doi:10.1016/j.procir.2017.03.168

and wettability of the AZ31 magnesium alloy. Cryogenic machining was used to obtain the formation of a featureless layer in the machined sub-surface, as well as the strategy of modifying the feed rate was used for controlling the surface wettability.
In-vitro degradation tests together with potentyodynamic polarization curves showed an ennobled corrosion behavior for the cryogenic and feed rate optimized machined samples.
The obtained results clearly demonstrated that the careful choice of the process parameters promoted a synergistic effect that can be exploited in increasing the service-life of magnesium biodegradable implants.

2. Experimental

2.1. Material

The material under investigation was the commercial available AZ31B magnesium alloy that was supplied in form of bars of 30 mm of diameter and 500 mm of length.

2.2. Machining tests

The machining tests were conducted on a Mori Seiki NL 1500™ CNC lathe equipped with a special designed line assembled to fulfil the cryogenic cooling. The cryogenic fluid used in the tests was Liquid Nitrogen (LN2), supplied to the cutting zone from a high pressure storage Dewar through a vacuum insulated pipe.

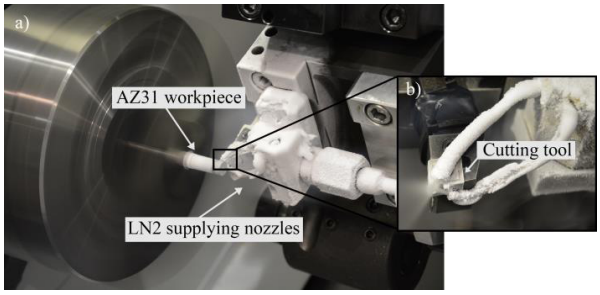

Fig. 1. a) experimental set-up for the cryogenic turning of the AZ31 samples; b) magnified photo of the liquid nitrogen delivery apparatus.

Two copper nozzles with an internal diameter of 0.9 mm were used to direct simultaneously the LN2 towards the tool flank and rake faces to improve its cooling capacity, as shown in Fig. 1. The adopted cutting tool was a semi-finishing insert VCEX110301LF1125 with a radius of 0.1 mm supplied by Sandvik Coromant™.
The values of the cutting speed (Vc) adopted for the tests was 100 m/min and was chosen on the basis of a literature study [6]. The depth of cut (d) was maintained constant and equal to 0.25 mm in order to achieve a semi-finishing cutting condition. The machining tests were performed under dry and cryogenic conditions.
The experimental plan for the machining tests is reported in Table 1. In the case of cryogenic cooling, different feed rate values were adopted namely 0.1 mm/rev, 0.05 mm/rev and 0.01 mm/rev.

Table 1. Experimental plan for the machining tests.

Feed rate (mm/rev)	Cooling condition	Cutting speed (m/min)	Depth of cut (mm)
0.1	Dry	100	0.25
0.1	Cryogenic	100	0.25
0.05	Cryogenic	100	0.25
0.01	Cryogenic	100	0.25

2.3. Microstructural and mechanical characterization

Metallurgical AZ31 Mg samples were cut from the machined cylinders. After cold mounting, grinding and polishing, acetic and picric acid aqueous solution was used as the etchant to reveal the grain boundaries. The microstructure observations were conducted using a Leica DMRE™ optical microscope equipped with a high definition digital camera and FEI QUANTA 450™ scanning electron microscope.Vickers micro-hardness measurements were carried out using a Leitz Durimet™ micro-hardness tester with a load of 470 mN for 30 s; five values were recorded for measurement and then the average value calculated. In order to investigate the effect of cooling condition on the micro-hardness values, measurements were taken every 30 μm from the machined surface to a depth of 120 μm.

2.4. Electrochemical tests

The electrochemical behavior was studied using a standard three electrodes cell, where the AZ31 machined samples were the working electrode, a saturated Calomel electrode (SCE) the reference electrode, and a platinum electrode the counter electrode. An Amel™ 2549 potentiostat was used for the electrochemical tests. The potentiodynamic polarisation curves were obtained applying a potential from -2 V to -1.3 V at a scan rate of 0.5 mVs^{-1}. The potentiodynamic polarization curves were obtained through testing in Simulated Body Fluid (SBF) solution, whose composition was 1.5881 g NaCl, 0.0709 g di $NaHCO_3$, 0.0492 g $Na_2HPO_4*7H_2O$, 0.0617 g di $MgCl_26H_2O$, 0.0746 g KCl, 0.0171 g di $CaSO_4*H_2O$, 0.0403 g $CaCl_2$, distilled water at 1 L, at body temperature (37±1°C), in order to reproduce the human body conditions. The corrosion potential (Ecorr) and the corrosion current density (Icorr) were determined from the polarization measurements using the Tafel extrapolation method, according to the ASTM G5-14 standard. The potentiodynamic polarization curves were repeated three times in order to assure the results reproducibility.

2.5. Contact angles measurements

The measure of the contact angle to evaluate the wettability of the machined samples was carried out applying a static sessile drop technique. The used experimental apparatus consisted of a horizontal stage used to place the sample, which allowed to be adjusted in the z-directions, a micrometer syringe to form a liquid drop, a halogen and intensity adjustable light source to illuminate the sample, and a Prosilica GT™ camera for the images acquisition. Before measuring, the samples were

cleaned in an ultrasonic bath for 15 min to remove any residual. Surface topography examinations were performed using a SensofarPlu-Neox™ optical 3Dprofiler with a resolution of less than 20 nm on the optical Z-axis. A liquid droplet of distilled water characterized by a volume of 10 µL was used. In order to investigate the effect of machining process parameters on wettability, the liquid droplet was fall on the lateral surface of the cylindrical sample. Tests was conducted at room temperature (25°C); each experiment was repeated eight times and the experimental results were taken as the mean value to assure reproducibility.

2.6. Evolved hydrogen gas measurements

Evolved hydrogen gas measurements were performed in order to evaluate the corrosion rate of machined samples exposed to the SBF solution whose composition is described in § 2.4. The hydrogen produced by the machined sample was collected by a funnel, located just above the sample, and then into a burette, placed over the funnel. The amount of evolved hydrogen was determined by measuring the displacement of the solution level in the burette. All of the test equipment was placed in a climatic chamber that assured a constant temperature of 37 ± 1°C.

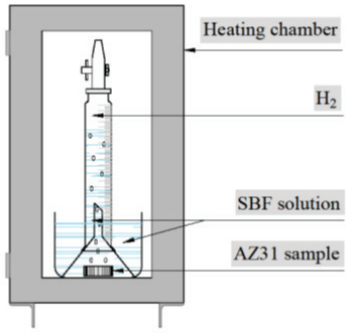

Fig. 2. Sketch of the experimental apparatus built up to measure the volume of hydrogen involved.

A schematic representation of the experimental apparatus designed for the evolved hydrogen gas measurements is shown in Fig. 2. The tests lasted 24 hours and the hydrogen evolution rate was calculated in ml*cm^{-2}. SEM investigations of the corroded surfaces were performed after tests.

3. Result and discussions

3.1. Microstructure and micro-hardness results

The microstructure of the AZ31 sample in the as-delivered state is shown in Fig. 3.a). The grain boundaries are clearly visible throughout the sample, even if the presence of some heavily deformed grains due to the sample preparation is noticeable.

The microstructure of the samples after dry and cryogenic machining is shown in Fig. 3.b) and c). In both cases, the area near the machined surface presents a significant Severe Plastic Deformed (SPD) layer, whose extension is increased in the case of the cryogenic machined sample.

It is worth to note that a SPD layer is noticeable also in the case of dry machining, oppositely to the available literature records on this topic [6]. These SPD layers are significantly affected by the presence of twins, in a higher amount compared to the initial microstructure.

On the top layer of the sample of Fig. 3.c), it can be noticed the presence of a featureless layer in which grain boundaries are no longer visible at this magnification. Similar evidences were reported in previous studies about machining of magnesium alloys [4,6]. This peculiar behaviour can be attributed to the large plastic deformation together with the suppression of heat due to the spraying of liquid nitrogen during machining.

To confirm the presence of such featureless layer, SEM investigations of the top layer of the cryogenic machined sample were carried out: the images of Fig. 4. confirm that the grain boundaries are not visible in such layer.

The effect of cooling strategies on micro-hardness profiles was investigated and results are reported in Fig. 5.

The cryogenic machined sample presents the highest micro-hardness values up to a distance of 90 µm from the machined surface. Such evidence appears to be coherent with the microstructures reported in Fig. 3.c, in which an extended work-hardened layer is clearly visible.

On the other hand, the dry machined sample shows a hardness comparable to the one of the as-delivered material: this can be attributed to the fact that the extension of the layer influenced by the machining process was less than 30 µm, which is the first point appreciable with the micro-hardness measurements.

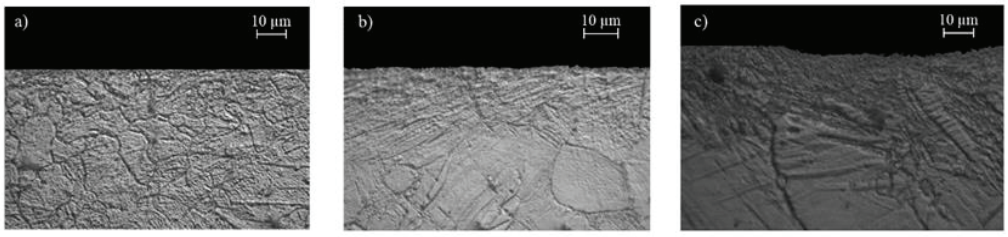

Fig. 3. Microstructure of the AZ31 samples machined with a feed rate equal to 0.1 mm/rev: a) as-delivered; b) after dry machining; c) after cryogenic machining.

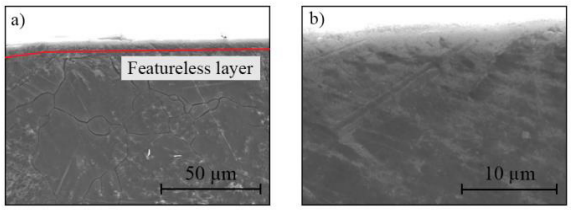

Fig. 4. SEM picture of the microstructure formed on the cryogenic machined sample: a) near the machined surface (200X magnification); b) zone included in the red dotted line of image a) (5000X magnification).

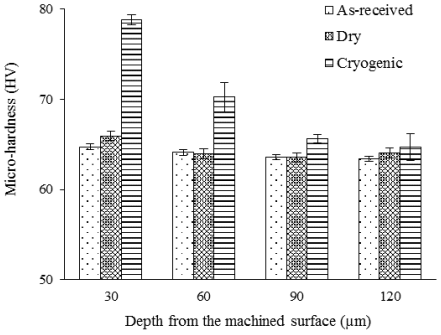

Fig. 5. Micro-hardness values under the machined surfaces.

3.2. Corrosion behaviour

The effect of the machining cooling strategies on the corrosion behaviour is reported in Fig. 6.a) in which the comparison between the investigated conditions is shown. Table 2 summaries the electrochemical data obtained from Fig 6.

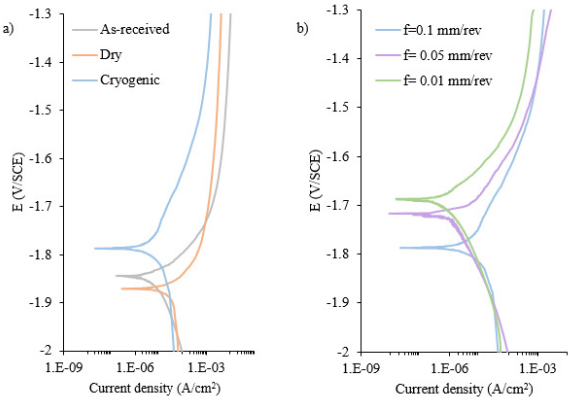

Fig. 6. Potentiodynamic polarisation curves for the AZ31 samples in SBF solution at 37°C: a) samples machined with different cooling strategies; b) samples machined under cryogenic cooling at different feed rates.

The tests results indicate that the corrosion rate of the as-delivered sample was comparable to that of the dry machined one and both are worse than the cryogenic machined sample. In the latter case, a decrease in the corrosion current of an order of magnitude was achieved.

Table 2. Electrochemical corrosion data.

Material condition		Ecorr (V/SCE)	Icorr (µA/cm²)
As delivered		-1.84	10
Feed rate (mm/rev)	Cooling condition		
0.1	Dry	-1.87	20
0.1	Cryogenic	-1.79	2
0.05	Cryogenic	-1.72	1.5
0.01	Cryogenic	-1.69	1

Overall, the corrosion curve of the cryogenic machined sample was shifted towards lower current density values compared to the other conditions. The corrosion data show that even if the dry machined sample presents an altered microstructure at the machined surface, especially if compared to the as-delivered one, its corrosion properties are slightly worse.

To give an explanation to such behaviour, it must be noted that the corrosion properties of the magnesium alloys mainly depend on crystallographic defects, such as grain boundaries, dislocations and twins, and on intermetallic particles, which are typically (Al,Mn) compounds. All of the aforementioned features are present in the as-delivered sample (see Fig. 7). The crystallographic defects preferentially corrode due to their chemical activity higher than the one of the bulk material, while the intermetallic particles act as a preferential site of galvanic corrosion. Since such features evolve during a surface deformation process, their contributions have to be considered with the respect to the corrosion resistance. Furthermore, the corrosion performances are slightly worsened when the grain size are over-refined, as shown in [7], where the ZK60 potentiodynamic polarization curves under two different conditions, namely the as-delivered state and after three ECAP passes, proved that the corrosion properties of the latter were almost the same even if the grain size was reduced down to 600 nm. The same results were achieved in [8], where EACP was applied to both pure magnesium and wrought ZM21 alloy.

Such non-monotonous relationship between the AZ31 grain size and its corrosion behaviour can be explained as follows: when a magnesium alloy has relatively large grains, the applied deformation introduces crystallographic defects such as grain boundaries, twins and dislocations and thus contribute to reduce the size of the intermetallic particles by dissolving them in the defects. In this case, the corrosion rate decreases as the grain refines.

.

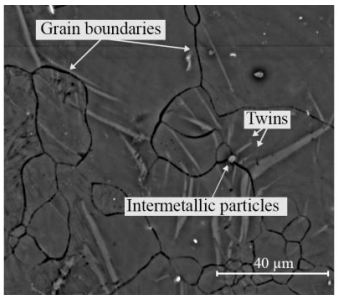

Fig. 7. SEM image of the as-delivered AZ31 showing the presence of crystallographic defects and intermetallic compounds.

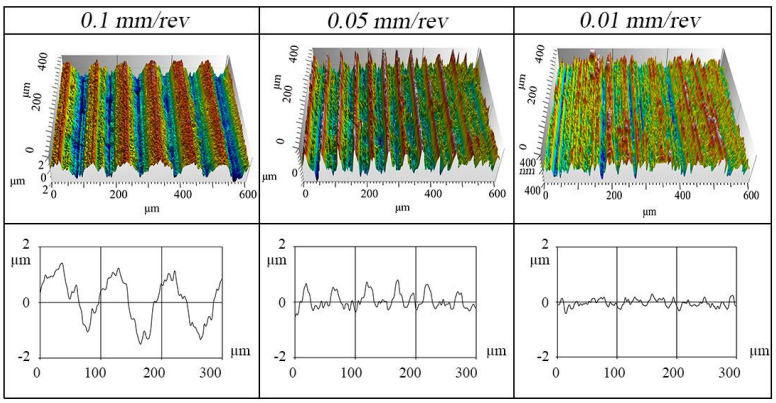

Fig. 8. 3D topographies (on the top) and 2D profiles (on the bottom) of the samples machined under cryogenic cooling at different feed rates.

After the grains become small enough and most particles are dissolved in the defects, a further grain refinement can only increase the densities of the crystallographic defects without further reducing the amount of intermetallic particles. Consequently, the alloy corrosion rate increases with further grain refinement.

These observations are in accordance with the microstructural results here presented: in the case of the dry machined sample, the surface layer is characterized by a significant decrease in the grain size compared to the as-delivered microstructure. The cryogenic machined sample, instead, presents a featureless layer in which the grain boundaries are not visible and the increase of the corrosion resistance can be therefore ascribed to that.

Based on these results, it was decided to focus on the investigation of the influence of the feed rate in the case of cryogenic machining.

3.3. Wettability

The effect of varying the feed rate has the major influence on the machined surface topography, which, in turn, is one of the main factors influencing the surface wettability.

As can be seen from the 3D topographies of Fig. 8., the feed rate change led to very different surfaces characterized by different surface roughness: as it increased rougher surfaces are produced.

The 2D profiles of Fig. 8. show that the feed rate value corresponds to the distance between two subsequent peaks: this is why, as the feed rate decreases, the number of feed marks increases in a given area.

A clear relationship between the water contact angle and the feed rate and, as a consequence, between the contact angle and the surface roughness values, were found and are plotted in Fig. 9.

Compared to the original experimental plan of Table 1, additional samples were machined with a feed rate equal to 0.02 mm/rev and 0.2 mm/rev for a better comprehension of the dependence of the contact angle on the feed rate. As can be seen from the graph in Fig. 9., the feed rate effect is appreciable only below 0.1 mm/rev.

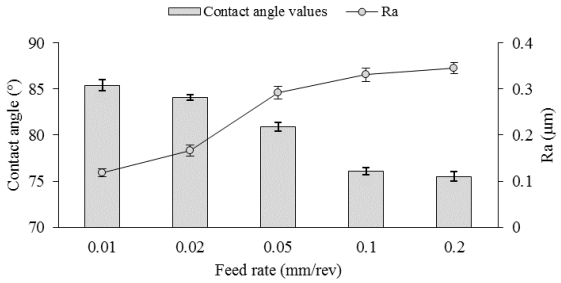

Fig. 9. Influence of the feed rate on the static water angle.

As a matter of fact, the contact angles of the samples machined at a feed rate of 0.1 mm/rev and 0.2 mm/rev are quite similar. Whereas, as the distance between two consecutive peaks becomes smaller than 0.1 mm, the contact angle is influenced by the feed rate: below this feed rate value, it can be stated that a lower feed rate increases the material hydrophobicity. The opposite trend is highlighted for the surface roughness: higher surface roughness induced lower contact angles. Both evidenced relationship can be explained by the fact that an increase of the feed marks density results in a decrease of the area fraction of the solid–liquid contact, which, according to the Cassie-Baxter model, decreases the water droplet contact angle.

Fig. 10 a) and b) shows the comparison of water droplets on the surface machined at feed rates of 0.01 and 0.2 mm/rev, which correspond to the leftmost and rightmost points in Fig. 9.

From the biological point of view, a high surface wettability is desirable because it promotes the material-tissue interactions leading to a rapid growth of apatite and better crystallization [9]. From the corrosion point of view, more hydrophobic surfaces are desirable because the interaction with the external environment is minimized [10]. In the case of magnesium alloys, whose poor corrosion resistance represents the major limit, the second aspect can be privileged and wettability can be seen as a characteristic to be correlated to the material tendency to corrode inside the human body.

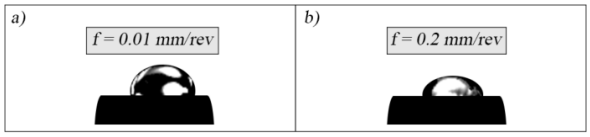

Fig. 10. Image of the water droplet fall on: a) sample machined in cryogenic condition and with a feed rate of 0.01 mm/rev; b) sample machined in cryogenic condition and with a feed rate of 0.2 mm/rev.

To confirm this, Fig. 6.b) shows the potentiodynamic polarization curves obtained for the sample machined under cryogenic cooling at different feed rates.
As the feed rate decreases, the corrosion curves are shifted towards higher potentials.
An increase of the corrosion potential of 0.1 V together with a decrease of the current density of 1 $\mu A/cm^2$ were achieved for the sample characterized by the lowest wettability.
As a matter of fact, the sample machined with a feed rate of 0.01 mm/rev presented the best corrosion properties among all the investigated conditions. The sample machined with a feed rate of 0.05 mm/rev lied in between.
This suggests that an increase in hydrophobicity allows a better corrosion behaviour. In summary, the creation of a surface characterized by a reduced wettability can be used as a strategy for improving the corrosion properties of magnesium alloys. This can be achieved by modifying the feed rate during the finishing operations of the machining process.

3.4. In vitro degradation

The overall observations are confirmed by the results of the hydrogen gas evolution reported in Fig. 11.a).
The dry machined sample presented an increase up to 60% in the formation of hydrogen if compared to the cryogenic machined ones.
Besides this, the latter were characterized by a less sever attack in correspondence of the zone near the machined surface as highlighted in the comparison of Fig. 11 b) and c).

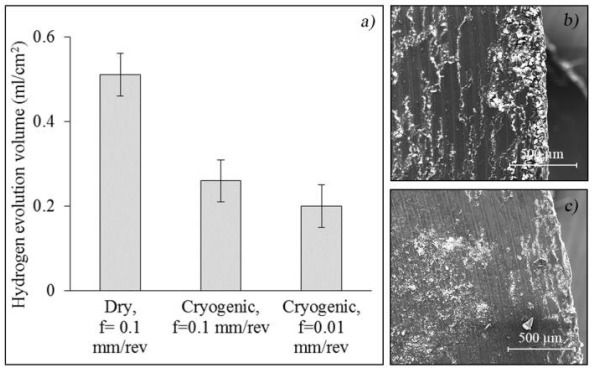

Fig. 11. a) Volume of evolved hydrogen; b) SEM image of the corroded surface of the sample machined in dry condition and with a feed rate of 0.1 mm/rev after the hydrogen evolution test; c) SEM image of the corroded surface of the sample machined in cryogenic condition and with a feed rate of 0.01 mm/rev after the hydrogen evolution test.

As expected, the lowest gas formation characterized the sample machined under cryogenic cooling at a feed rate equal to 0.01 mm/rev.

4. Conclusions

The present study showed that the corrosion behaviour of the AZ31 magnesium alloy could be effectively modified by varying the machining parameters.
Both dry and cryogenic machining could affect the microstructure of the machined sample, but only in the latter case a featureless layer was formed.
The feed rate change affects the surface roughness and, as a consequence, influences the wettability of the surfaces in terms of reduction of the water contact angle.
An enhancement of the AZ31 corrosion behaviour was achieved by combining the aforementioned optimized machining parameters. The adoption of cryogenic cooling together with feed rates as low as 0.01 mm/rev represents an efficient strategy to improve the AZ31 corrosion behavior.

References

[1] Klocke F, Schwade M, Klink A, Veselovac D, Kopp A. Influence of Electro Discharge Machining of biodegradable magnesium on the biocompatibility. Procedia CIRP 2013;5:88–93.
[2] Ratna Sunil B, Sampath Kumar TS, Chakkingal U, Nandakumar V, Doble M, Devi Prasad V, Raghunath M. In vitro and in vivo studies of biodegradable fine grained AZ31 magnesium alloy produced by equal channel angular pressing. Mater Sci Eng C 2016;59:356–367.
[3] Denkena B, Lucas A. Biocompatible magnesium alloys as absorbable implant materials adjusted surface and subsurface properties by machining processes. CIRP Ann - Manuf Technol 2007;56:113–116.
[4] Dinesh S, Senthilkumar V, Asokan P, Arulkirubakaran D. Effect of cryogenic cooling on machinability and surface quality of bio-degradable ZK60 Mg alloy. Mater Des 2015;87:1030–1036.
[5] Zhang P, Lindemann J. Effect of roller burnishing on the high cycle fatigue performance of the high-strength wrought magnesium alloy AZ80. Scr Mater 2005;52:1011–1015.
[6] Pu Z, Puleo DA, Dillon OW, Jawahir IS. Controlling the biodegradation rate of magnesium-based implants through surface nanocrystallization induced by cryogenic machining. In: Sillekens WH, Agnew SR, Neelameggham NR, Mathauudhu SN, editors. Magnesium Technol. New York: John Wiley & Sons Inc; 2011. p.637–642.
[7] Mostaed E, Hashempour M, Fabrizi A, Dellasega D, Bestetti M, F. Bonollo, Vedani M. Microstructure, texture evolution, mechanical properties and corrosion behavior of ECAP processed ZK60 magnesium alloy for biodegradable applications. J Mech Behav Biomed Mater 2014;37:307–322.
[8] Qiang G, Mostaed E, Zanella C, Zhentao Y, Vedani M. Ultra-Fine Grained Degradable Magnesium for Biomedical Applications. Rare Met Mater Eng 2014; 43:2561–2566.
[9] Pietrikova A, Lukacs AP, Jakubeczyova D, Ballokova B, Potencki J, Tomaszewski G, Pekarek J, Prikrylova K, Fides M. Surface analysis of polymeric substrates used for inkjet printing technology. Circuit World 2016; 42:9–16.
[10] Liu Y, Yao W, Yin X, Wang H, Han Z, Ren L. Controlling Wettability for Improved Corrosion Inhibition on Magnesium Alloy as Biomedical Implant Material. Adv Mater Interfaces 2016;3:1500723.